High dynamic range ultrasound beamforming using deep neural networks

Luchies, Adam, Byram, Brett

Adam Luchies, Brett Byram, "High dynamic range ultrasound beamforming using deep neural networks," Proc. SPIE 10955, Medical Imaging 2019: Ultrasonic Imaging and Tomography, 109550P (15 March 2019); doi: 10.1117/12.2514185

SPIE.

Event: SPIE Medical Imaging, 2019, San Diego, California, United States

High dynamic range ultrasound beamforming using deep neural networks

Adam Luchies and Brett Byram

Vanderbilt University, Department of Biomedical Engineering, Nashville, TN, USA

ABSTRACT

We investigated using deep neural networks (DNNs) to beamform ultrasound images with high dynamic range targets. The DNNs operated on frequency domain data, the inputs consisted of the separated in-phase and quadrature components observed across the aperture of the array, and the outputs of the DNNs had the same structure as the inputs. We compared several methods for generating training data, including training with hypoechoic and anechoic cysts. All training data was generated using a linear ultrasound simulation tool. The results demonstrate the potential for using DNN beamformers to extend the dynamic range of ultrasound beamforming.

Keywords: Ultrasound beamforming, neural networks, off-axis scattering, hyperechoic cysts, hypoechoic cysts, anechoic cysts

1. INTRODUCTION

The beam of an ultrasound imaging system is commonly characterized by main lobe width and peak-side-lobe level. Ideally, the main lobe would be made as narrow as possible and the side lobes as small as possible. However, these beam characteristics usually compete in an engineering tradeoff. Reducing the main lobe width leads to higher side lobes and reducing side lobe levels leads to increased main lobe width.

In general, side lobes decrease image contrast and are particularly problematic for hyperechoic or hypoechoic cysts. For these kinds of targets, side lobes cause signals from regions of weak scattering to be masked by signals from nearby regions of strong scattering. For example, the signals from lung tissue often mask the signals from adjacent myocardial tissue, which complicates cardiac ultrasound examination. In a second example, strong off-axis scattering can complicate the differentiation of simple and complex cysts.

The high dynamic range targets like those described cause issues for delay-and-sum (DAS) beamforming. However, they often pose an even greater challenge for many of the advanced adaptive beamformers that have been developed by the ultrasound community. For example, when imaging strong point targets, many advanced beamforming methods suffer from a dark region artifact that does not affect DAS.[1] Dei et. al. showed that few advanced beamforming methods were able to match the contrast dynamic range already provided by standard DAS beamforming and some advanced beamformers even created contrast curves that were not linear as a function of intrinsic contrast.[2] Attempts have been made to extend the dynamic range of ultrasound beamformers. For example, Schlunk et al. developed an iterative version of the aperture domain model image reconstruction (ADMIRE) beamformer with the goal of extending the contrast dynamic range of ADMIRE.[3–5]

Recently, we developed a deep neural network (DNN) based beamforming method for improving ultrasound image quality.[6] We showed that it was possible to train neural networks using simulated data and these networks generalized well enough to achieve image quality improvements in physical phantom and *in vivo* scans.[7] Using phantom and *in vivo* studies, we were able to improve image contrast by reducing the effect of off-axis scattering. We also showed that this DNN beamforming method is robust to noise.[8] The goal of this work was to study the problem of high dynamic range targets and to train DNN beamformers to improve image quality for these these kinds of targets.

Send correspondence to adam.c.luchies@vanderbilt.edu

Medical Imaging 2019: Ultrasonic Imaging and Tomography, edited by Brett C. Byram, Nicole V. Ruiter, Proc. of SPIE Vol. 10955, 109550P · © 2019 SPIE
CCC code: 1605-7422/19/$18 · doi: 10.1117/12.2514185

2. METHODS

The DNN beamformer studied in this work has been described previously.[9] This type of DNN beamformer consists of a set of deep neural networks (DNNs) that operate on frequency domain data and a different DNN is trained for each frequency. A short-time Fourier transform (STFT) converted channel data into the frequency domain and the depths were processed independently. After DNN processing, an inverse short-time Fourier transform (ISTFT) was used to convert back to the time-domain. The STFT window length was one pulse length, a rectangular window was used, and the STFT window overlap was 90%.

The training data was generated using Field II.[10,11] The simulated transducer was modeled after an ATL L7-4 (38 mm) linear array probe. The transmit focus was 7 cm, the center frequency was 5.208 MHz, the pitch was 298 μm, and a 65 element element sliding window was used during transmit and receive.

2.1 Hypoechoic cyst training data

In order to train DNN beamformers for high dynamic range targets, we introduce a new method for generating training data using simulated cysts with varying intrinsic contrast. The first step was to generate two separate channel data sets: one for the background region (i.e., an anechoic cyst) and a second for the inside cyst region (i.e., an anechoic background) as shown in Fig. 1. These two channel data sets were combined to form a data set for a cyst with a specified intrinsic contrast so that three channel data sets were available: anechoic cyst data, anechoic background data, and hypoechoic cyst data.

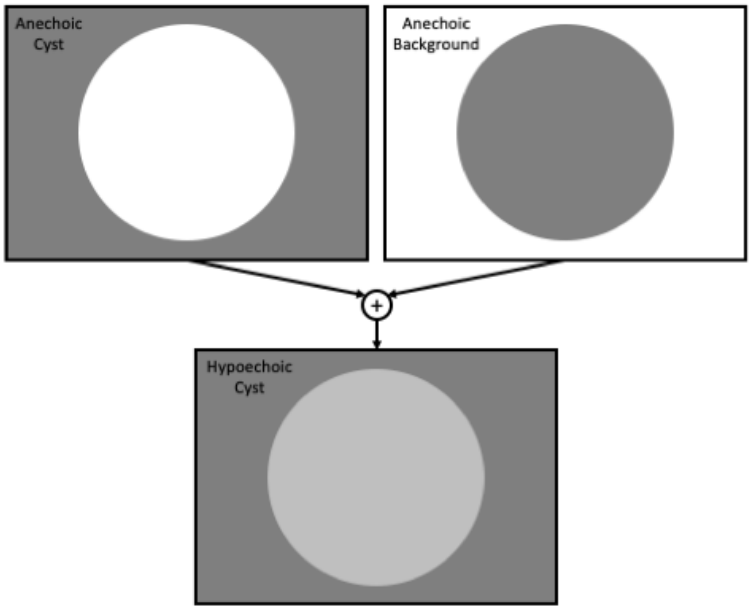

Figure 1. Method for generating data for a hypoechoic cyst using an anechoic cyst and anechoic background.

Training data for high dynamic range DNN beamformers were generated using these three channel data sets as shown in Fig. 2. First, training data was generated from the inside of the cyst using the hypoechoic cyst channel data as the training input and the anechoic background data as the training output as shown in Fig. 2 (a). Both data sets were transformed into the frequency domain using a STFT. A circle was inscribed on the inside of the cyst. All STFT segments outside of this circle were discarded. The hypoechoic cyst STFT segments were used as the input training examples and the anechoic background STFT segments were used as the matched output training examples.

Second, training data was generated from the outside of the cyst by using the hypoechoic cyst channel data as the training input and the anechoic cyst data as the training output as shown in Fig. 2 (b). Both data sets were transformed into the frequency domain using a STFT. A circle was inscribed on the inside of the cyst. All STFT

segments that were inside the circle were discarded. The hypoechoic cyst STFT segments were used as the input training examples and the anechoic cyst STFT segments were used as the matched output training examples. The number of training examples from outside the cyst was made to be equal to the number of training examples from inside the cyst that were created in the previous step. The STFT segments from outside the cyst that were closest to the the cyst were kept and the remaining were discarded.

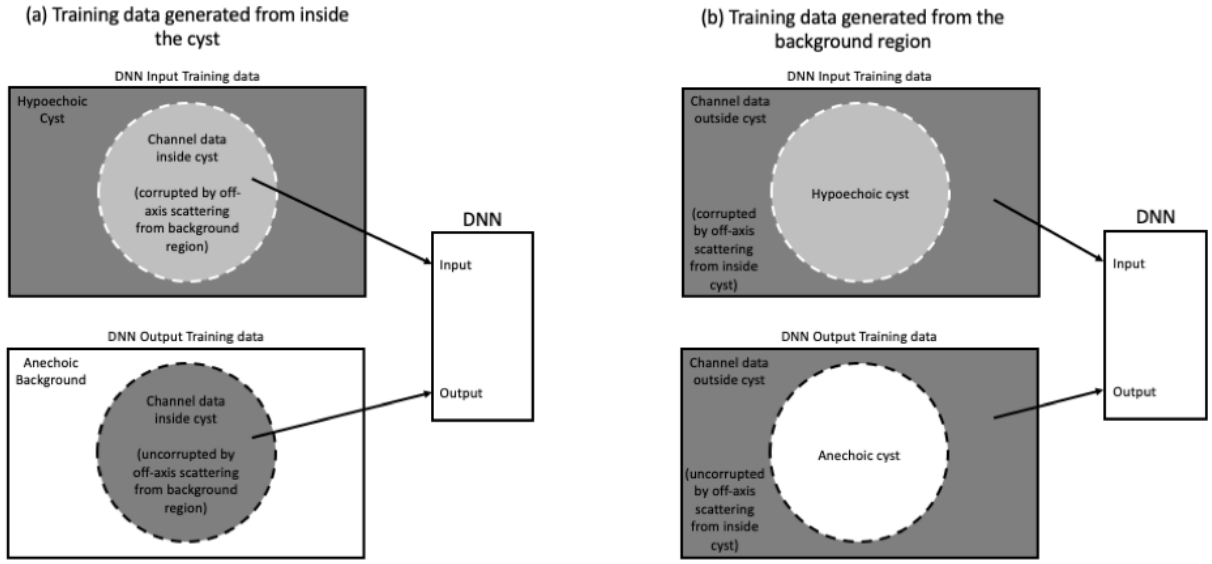

Figure 2. Method for generating training data using hypoechoic cysts.

2.2 Anechoic cyst training data

To demonstrate that importance of using a high dynamic range training data generated from targets similar to hypoechoic cysts, we also generated a training data set using only anechoic cysts. The channel data from an anechoic cyst was transformed into the frequency domain using a STFT. A circle was inscribed on the inside of the cyst. The STFT segments that were inside the circle were used as training inputs and the corresponding training outputs were vectors of zeros. The STFT segments that were on the outside of the circle were also used as training inputs and the corresponding training outputs were the same data as the input.

2.3 Neural networks

The DNNs were fully connected and the connections were feedforward. The number of hidden layers was in the range 5-10, the layer width was equal for all layers and was selected from the range 520-1040, and the dropout probability was selected from the range 0-0.5. The rectified linear unit was used as the activation function. Noise was added to the training data to help prevent overfitting.

2.4 Image quality metrics

Image quality was quantified using contrast ratio (CR) as

$$\mathrm{CR} = -20\log_{10}\left(\frac{\mu_{\mathrm{inside}}}{\mu_{\mathrm{background}}}\right), \tag{1}$$

contrast-to-noise ratio (CNR) as

$$\mathrm{CNR} = 20\log_{10}\left(\frac{|\mu_{\mathrm{background}} - \mu_{\mathrm{inside}}|}{\sqrt{\sigma^2_{\mathrm{background}} + \sigma^2_{\mathrm{inside}}}}\right), \tag{2}$$

and speckle signal-to-noise ratio (SNRs) as

$$\text{SNRs} = \frac{\mu_{\text{background}}}{\sigma_{\text{background}}}, \tag{3}$$

where μ is the mean and σ is the standard deviation of the uncompressed envelope.

3. RESULTS

3.1 Hypoechoic cyst results

Fig. 3 shows example images of hypoechoic cysts for DAS, DNN beamformers trained with anechoic cysts, and DNN beamformers trained with hypoechoic cysts. Figs. 3 (a) and (d) show how DAS underestimated contrast relative to the intrinsic contrast of the cyst. Figs. 3 (b) and (e) show how the DNN beamformer trained with anechoic cysts overestimated contrast relative to the intrinsic contrast of the cyst. Figs. 3 (c) and (f) show how the DNN beamformer trained with hypoechoic cysts produced the contrast that was closest to that of the intrinsic contrast for the studied cysts. Comparison of the region on the inside of the cyst in Figs. 3 (c) and (f) with the same region in Fig. 3 (h) demonstrates how DNN beamformers trained with hypoechoic cysts recovered the speckle pattern for the scatterers on the inside of the cyst. In contrast, DAS and DNN beamformers trained with anechoic cysts distorted the speckle pattern for the scatterers on the inside of the cyst.

Fig. 4 demonstrates quantitatively that training with hypoechoic cysts produced the best estimates of intrinsic contrast. Clearly, DAS underestimated contrast and the DNN beamformer trained with anechoic cysts overestimated contrast.

3.2 Hyperechoic cyst results

A set of hyperechoic cysts were also studied and example images are shown in Fig. 5. Figs. 5 (a) and (d) show how energy from the hyperechoic cyst spreads into the adjacent regions of weaker scattering outside the cyst. Specifically, the hyperechoic cyst masks features of the target that are adjacent to the cyst. Figs. 5 (b) and (e) show how DNN beamformers trained with anechoic cysts suffer from a dark region artifact.[1] Figs. 5 (c) and (f) show how DNN beamformers trained with hypoechoic cysts have significantly reduced the dark region artifact and the boundaries of the cysts are much better dilineated compared to DAS.

Fig. 6 demonstrates quantitatively that training with hypoechoic cysts produced the best estimates of intrinsic contrast for hyperechoic cysts. Furthermore, these results show that DNN beamformers trained with hypoechoic cysts generalized well enough to improve estimation of intrinsic contrast in hyperechoic cysts. However, it should be noted that the background region speckle pattern in Figs. 5 (c) and (f) did not appear to match the speckle pattern in Fig. 5 (g). Based on the hypoechoic cyst results, we would expect that training with hyperchoic cyst training data would provide a way to recover the background region speckle pattern that was masked by off-axis scattering in the DAS images.

4. CONCLUSIONS

In this study, we described a method for training DNN beamformers for high dynamic range targets. We used hypoechoic cysts and trained DNN beamformers to map from a signal space corrupted by strong off-axis scattering to a corresponding signal space that was uncorrupted by strong off-axis scattering. We found that DNN beamformers trained using this method improved contrast estimation for the types of targets used to generate the training data, mainly hypoechoic cysts. We also found that these DNN beamformers generalized well enough to improve contrast estimation in a different kind of target, hyperechoic cysts, that were also affected by strong off-axis scattering.

ACKNOWLEDGMENTS

The authors would like to thank the staff of the Vanderbilt University ACCRE computing resource. This work was supported by NIH grants R01EB020040 and S10OD016216-01, and additionally by NSF award IIS-1750994.

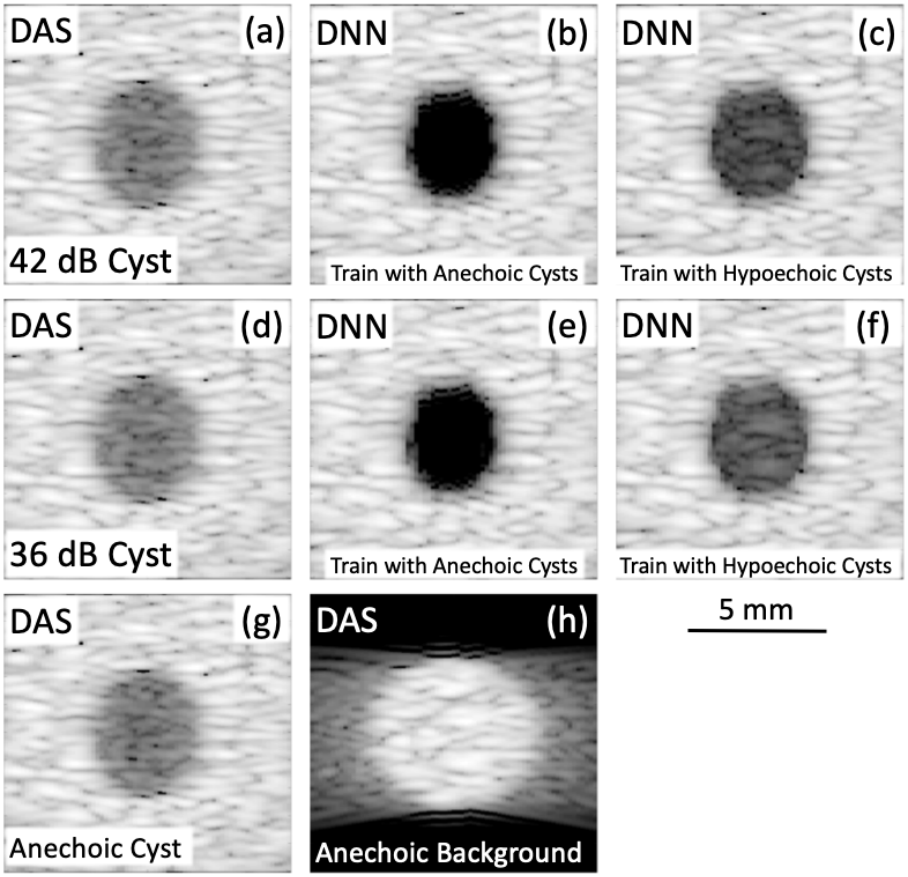

Figure 3. Examples of hypoechoic cysts for DAS, DNN beamformers trained with anechoic cysts, and DNN beamformers trained with hypoechoic cysts.

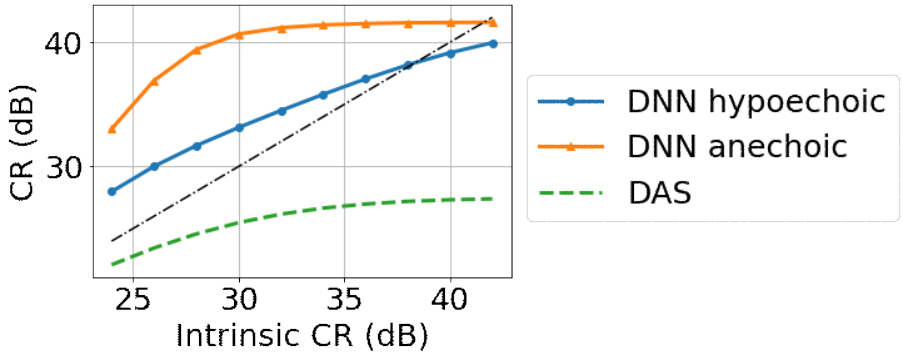

Figure 4. CR as a function of intrinsic CR for DAS, DNN beamformers trained with anechoic cysts, and DNN beamformers trained with hypoechoic cysts.

REFERENCES

[1] Rindal, O., Rodriguez-Molares, A., and Austeng, A., "The dark region artifact in adaptive ultrasound beamforming," *Proc. IEEE Ultrason. Symp.* (2017).

[2] Dei, K., Luchies, A., and Byram, B., "Contrast ratio dynamic range: A new beamformer performance metric," *Proc. IEEE Ultrason. Symp.* (2017).

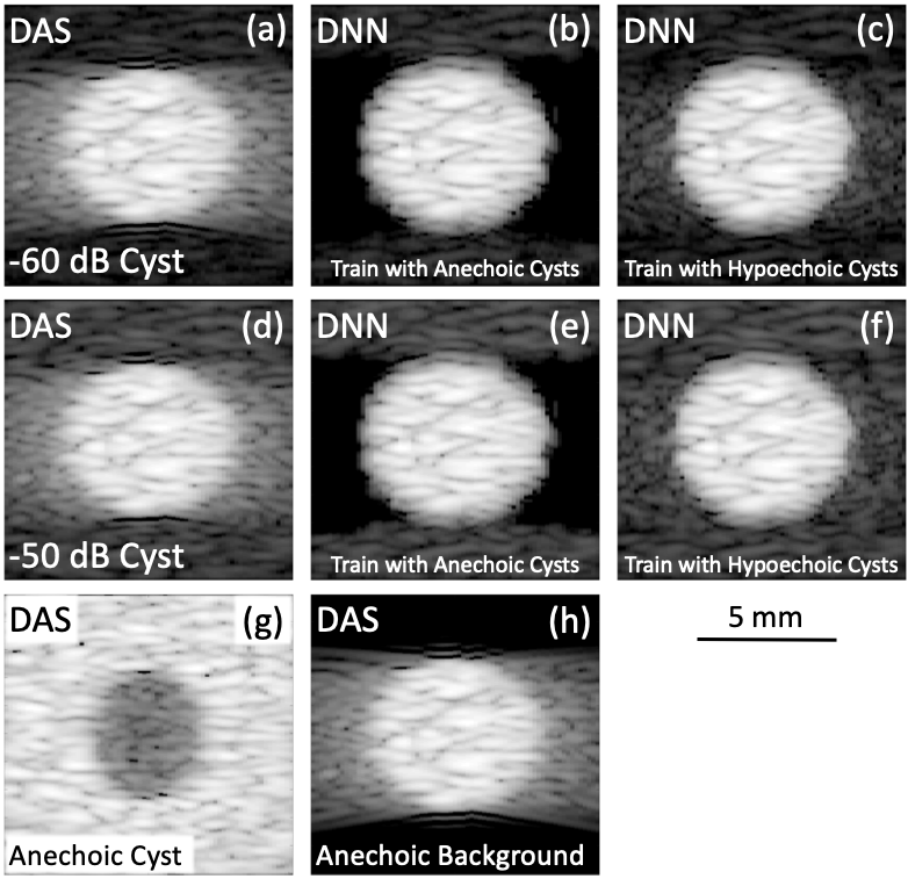

Figure 5. Examples of hyperechoic cysts for DAS, DNN beamformers trained with anechoic cysts, and DNN beamformers trained with hypoechoic cysts.

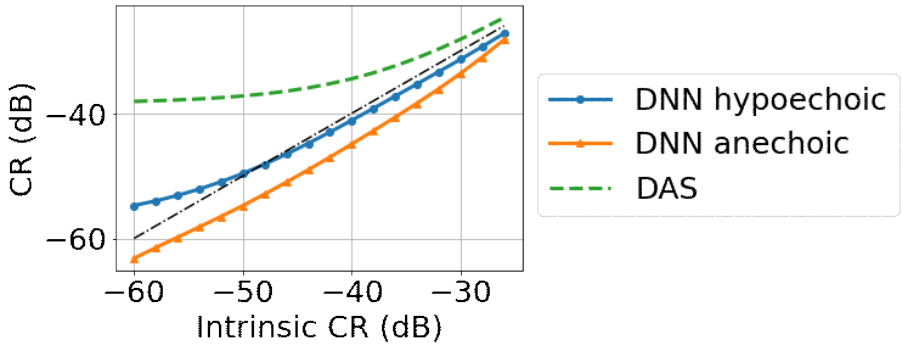

Figure 6. CR as a function of intrinsic CR for DAS, DNN beamformers trained with anechoic cysts, and DNN beamformers trained with hypoechoic cysts.

[3] Schlunk, S., Dei, K., and Byram, B., "Iterative admire for high dynamic range b-mode," *Proc. IEEE Ultrason. Symp.* (2018).

[4] Byram, B. and Jakovljevic, M., "Ultrasonic multipath and beamforming clutter reduction: A chirp model approach," *IEEE Trans. Ultrason. Ferroelectr. Freq. Control* **61**, 1377–1388 (2011).

[5] Byram, B., Dei, K., Tierney, J., and Dumont, D., "A model and regularization scheme for ultrasonic beamforming clutter reduction," *IEEE Trans. Ultrason. Ferroelectr. Freq. Control* **62**, 1913–1927 (2015).

[6] Luchies, A. and Byram, B., "Deep neural networks for ultrasound beamforming," *Proc. IEEE Ultrason. Symp.* (2017).
[7] Luchies, A. C. and Byram, B. C., "Deep neural networks for ultrasound beamforming," *IEEE Trans. on Med. Imag.* **37**, 2010–2021 (2018).
[8] Luchies, A. and Byram, B., "Suppressing off-axis scattering using deep neural networks," *Proc. SPIE* **10580**, 105800G (2018).
[9] Luchies, A. C. and Byram, B. C., "Training improvements for ultrasound beamforming with deep neural networks," *Phys. Med. Biol.* (in press).
[10] Jensen, J. A. and Svendsen, N. B., "Calculation of pressure fields from arbitrarily shaped, apodized, and excited ultrasound transducers," *IEEE Trans. Ultrason. Ferroelectr. Freq. Control* **39**, 262–267 (1992).
[11] Jensen, J. A., "Field: A program for simulating ultrasound systems," *Proc. Med. Biol. Eng. Comput.* **34**, 351–353 (1996).